

de Haas-van Alphen effect and the band structure of URh₃[†]

A. J. Arko, M. B. Brodsky, G. W. Crabtree, D. Karim, D. D. Koelling, and L. R. Windmiller
Argonne National Laboratory, Argonne, Illinois 60439

J. B. Ketterson

Northwestern University, Evanston, Illinois 60201
and Argonne National Laboratory, Argonne, Illinois 60439

(Received 14 July 1975)

We have performed measurements of the de Haas-van Alphen (dHvA) effect in the intermetallic compound URh₃, a material with a partially filled 5*f* shell. Complex dHvA spectra containing several frequencies were observed and Fourier analyzed with an on-line computer. Effective-mass measurements were made for several orbits and values as large as 5.3 were observed. Much of the data are consistent with a multiply connected surface whose shape is discussed. In addition to the dHvA experiments, a detailed band-structure calculation was performed using the nonflat relativistic-augmented-plane-wave formalism. The Fermi surface deduced from these calculations is in qualitative agreement with the experimental observation.

I. INTRODUCTION

Actinide metals and many intermetallic compounds display unusual electronic and magnetic properties which are attributed to itinerant 5*f* electrons in narrow 5*f* bands.^{1,2} In many cases a detailed knowledge of the band structure is essential in fully understanding the observed phenomena and gaining insight into the underlying physics. Yet, despite years of study, the band structures of actinide metals above thorium are not fully understood.

The exotic crystal structures of the pure actinide metals present formidable problems to the calculations of the band structure of these materials. As a result, most exploratory calculations have been performed for the high-temperature fcc and bcc phases with an emphasis on whether or not a band picture is appropriate for the *f* states.³ There are also severe experimental problems. The high chemical reactivity and numerous relatively-low-temperature phase transitions¹ make it difficult to obtain pure, unstrained single crystals. In addition, the effective masses associated with *f*-like levels can be rather high. These problems have precluded the possibility of a detailed comparison between band-structure calculations and hard experimental data such as those provided by de Haas-van Alphen (dHvA) measurements with the exceptions of⁴ Th and⁵ U.

By contrast, many actinide intermetallic compounds are relatively well behaved and thus can reduce the severe experimental and theoretical problems encountered in the pure metals. Moreover, the electronic and magnetic properties attributed to the itinerant 5*f* electrons are no less interesting in the compounds and are in many cases

even more exotic. One obtains the entire spectrum of narrow-band effects from simple transition-metal behavior ($\rho \propto T^5$ at low temperatures) through nearly magnetic phenomena (spin fluctuations, etc.) to ordered magnetic phenomena.⁶ Thus a study of the actinide intermetallic compounds presents an exciting prospect. This excitement is further enhanced by the ability to observe the de Haas-van Alphen effect in some of these intermetallics, which allows one to test the reliability of a band-structure calculation for a system containing itinerant *f* states.

URh₃ has been chosen as the first actinide intermetallic for study both because good samples can be prepared with relative ease and because it exhibits itinerant *f*-state character. URh₃ is a congruent-melting line compound having the cubic *L*1₂ (or ordered AuCu₃) structure. It is easily purified and good crystals are readily obtained by electron-beam zone refining. A sizeable body of evidence exists^{7,8} to indicate that the *f* states are itinerant (and thus manageable). The low-temperature resistivity increases as T^3 while the magnetic susceptibility is temperature independent. The electronic specific heat⁹ is relatively small ($\gamma=14$ mJ/°K²) for an actinide intermetallic, so effective masses should not be unmanageably large. Thus, while there are 5*f* states present, the electronic properties are not complicated by the nearly magnetic phenomena which will be the basis for future investigations. Furthermore, URh₃ provides an opportunity to examine the correlation of the actinide-actinide separation¹⁰ with magnetic and superconducting properties. On the plots representing this correlation, URh₃ falls well into the region that should be magnetic. Yet it is not. This can be attributed qualitatively to

the formation of a $d-f$ bond which is favorable¹¹ in this system. This could explain why URh₃ has a higher melting temperature¹² than ThRh₃.

In this paper we present the results of the dHvA measurements on URh₃ and propose a tentative Fermi-surface model. Band-structure calculations have been performed which agree with the gross features of the model although, as we will see, they do not yet indicate complete agreement. In Sec. II we present the experimental data, while the band-structure calculations are presented in Sec. III. These are then discussed in Sec. IV, where future work is suggested.

II. EXPERIMENT

A. Sample preparation

The compound was prepared by rf heating of the constituent materials in a silver boat in an inert atmosphere using 99.999% pure rhodium from High Purity Metals and 99.99% pure uranium. A rod of the specimen (5 cm long \times \approx 3 mm in diameter) was then electron-beam zone refined three times to form a single crystal and purify the bar. The vapor pressures of both constituent materials at the melting point of the compound (\approx 1700 °C) are sufficiently low so that the small evaporation causes no stoichiometry problems. A crystal having a residual-resistance ratio of 170 was obtained. (The measured Dingle temperature was 0.5 °K.) A small specimen (\approx 0.8 mm on a side) was cut from this crystal and etched to remove damage.

B. Measurements

Because of the large effective masses ($m^* > 5.0$ for some orientations) and relatively high Dingle temperatures (0.5 °K), it was necessary to use very large magnetic fields; these were provided by a 132-kGNb₃Sn superconducting solenoid. In addition, the amplitude of the dHvA signal was further increased by operating at temperatures below 0.4 °K using ³He evaporative cooling. Only the low-mass frequencies labeled γ and δ in Fig. 2 were observed in the initial runs below 70 kG and at 1.1 °K. The usual field-modulation technique was employed.¹³ The spectral content of the dHvA signal was analyzed by an on-line PDP-11/20 minicomputer programmed to perform fast¹⁴ or slow Fourier transforms; this capability proves to be absolutely essential when analyzing complex dHvA spectra. A complete set of measurements was made in the (100) and (110) planes.

The large effective masses in URh₃ are difficult to measure because the signal disappears very rapidly with increasing temperature. In many cases the signal was weak or absent above 1 °K,

where effective-mass measurements are normally made. To circumvent this problem, the masses reported here were measured at temperatures below 1 °K. Temperatures were determined by vapor pressure thermometry on the ³He producing the evaporative cooling. To avoid errors caused by the pressure drop in the ³He pumping line, a separate static line was used for the vapor-pressure measurements. The open end of a 0.026-in.-I.D. capillary tube was placed just above the level of ³He surrounding the sample in the tail of the cryostat. This capillary was soldered to the inner wall of the cryostat tail for a distance of several inches. At the point where the tail emerged from the bore of the magnet, the capillary was brought through the wall of the tail and connected to a 0.500-in.-I.D. stainless-steel tube. This tube extended from 1 to 77 °K; from 77 °K to room temperature the line was enlarged to 1 in. I.D. Pressures were measured at room temperature with a Texas Instruments Model 145 differential pressure gauge. Temperatures as low as 0.5 °K could be measured without making any thermomolecular pressure corrections, and all of our mass measurements were made in the range 0.55–1 °K. We found that the sample and ³He required about 1 min to come into thermal equilibrium after changing the temperature of the system. By allowing for this thermal time constant, the mass plots of $\ln(A/T)$ vs T were good fits to a straight line, and the resulting masses had errors of about 2%. The success of this technique in measuring masses as high as 5.3 emphasizes the importance of high fields and low temperatures for studies of actinide metals and compounds.

III. RESULTS AND DISCUSSION

A. Experimental Fermi surface

The cross-sectional areas in atomic units are shown as a function of orientation in Figs. 1 and 2. Table I lists the effective masses on the various branches. The disjointed frequency branches in Fig. 1 are highly suggestive of a multiply connected Fermi surface. The effective masses on these branches range from a minimum of 2.5 on the branch labeled α to the maximum measurable value of 5.3 near the extinction points of β_1 , in the (110) plane. The effective masses on the branches ν_1 , ν_2 , ζ , and ξ were probably larger than 5.3, but could not be measured because the signal was observable only at the lowest temperatures.

The branch labeled γ in Fig. 2 comes from a single sheet of Fermi surface and has the symmetry of the point Γ or R of the simple-cubic Brillouin zone (see Fig. 3 for symmetry labels). It has the lowest effective mass (\sim 0.5 at [100]) of

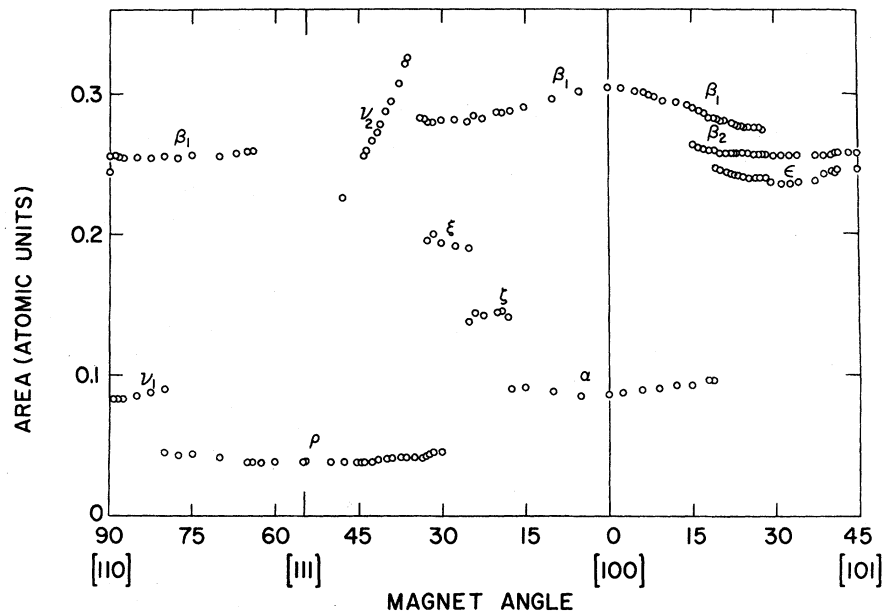


FIG. 1. Cross-sectional areas in atomic units for the large multiply connected pieces of Fermi surface in URh_3 .

all frequency branches in URh_3 and could be observed in fields as low as 10 kG at 1.1 °K.

The frequency branch δ is the lowest frequency in the URh_3 spectrum but has a mass at [100] of 0.61, somewhat larger than γ . It consists of two

branches which because of low anisotropy could not be clearly resolved. Because of this, the symmetry of δ has not been determined, although with the help of the band-structure calculations (to be discussed) the most likely symmetry is

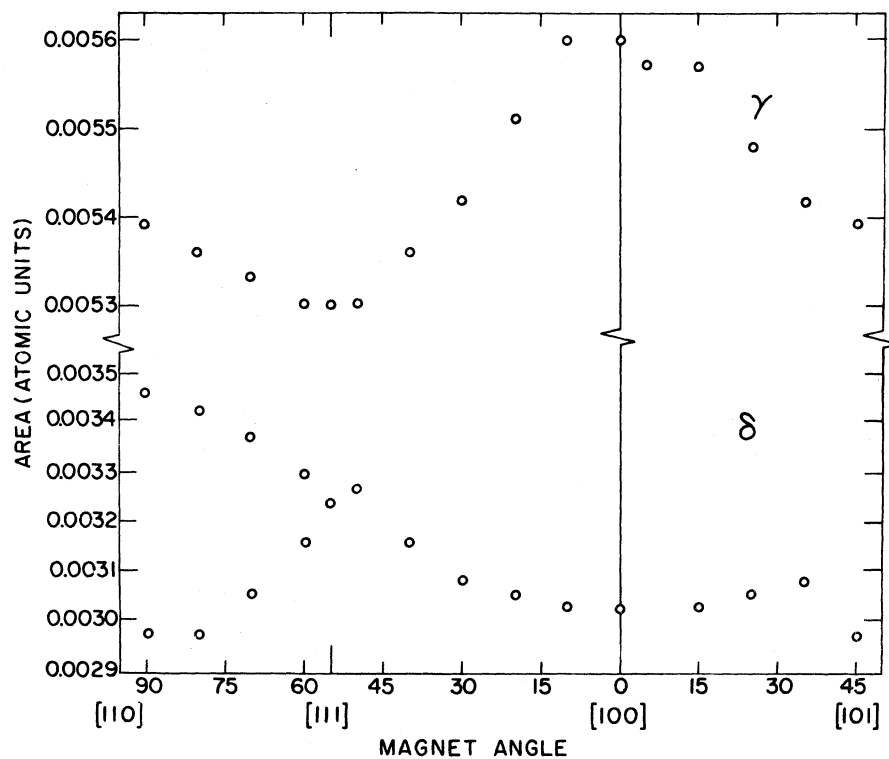


FIG. 2. Cross-sectional areas for the small closed pieces of Fermi surface in URh_3 .

TABLE I. Effective masses in URh₃.

Orbit	Plane	Degrees from [100]	Effective mass m^*
α	(100)	0°	2.50
γ	(100)	0°	0.49
δ	(100)	0°	0.61
β_1	(100)	0°	3.01
β_1	(100)	12.5°	3.16
β_1	(100)	18.5°	3.30
β_1	(100)	24.5°	3.70
β_2	(100)	18.5°	5.12
β_2	(100)	24.5°	4.03
β_2	(100)	30°	3.88
β_2	(100)	34.5°	3.71
β_2	(100)	45°	3.73
ϵ	(100)	34.5°	3.66
ρ	(110)	70°	2.35
ρ	(110)	54.5°	2.22
ρ	(110)	33°	3.00
β_1	(110)	80°	3.80
β_1	(110)	70°	5.00
β_1	(110)	65°	5.25
β_1	(110)	28°	4.01

that of Δ .

As stated above, the data in Fig. 1 are such that the Fermi surface almost certainly must be open. The large slowly varying branches β_1 and β_2 appear to be due to a set of "ellipsoids" connected to each other via a neck. The branch ν_1 could be such a neck frequency, so that the neck direction is along [110]. The symmetry of the ellipsoids cannot be determined from the data. However, as will be seen below, the calculated bands, while not agreeing in detail with the data, do indicate that for any electron potential used the largest piece of Fermi surface is centered at M . Thus if we place our large ellipsoids (nearly spherical) at M and connect them by [110] necks we obtain a Fermi surface topologically similar to the model shown in Fig. 3. (For clarity we have not included the small closed Γ -centered surface or the even smaller surfaces possibly located at Δ .) Three such ellipsoids are then contained in the Brillouin zone and fill about $\frac{1}{2}$ the volume of the zone. A Fermi surface having the topology shown in Fig. 3 is open along [110] and [100]. Magnetoresistance measurements were done at 70 kG and 1.1°K.

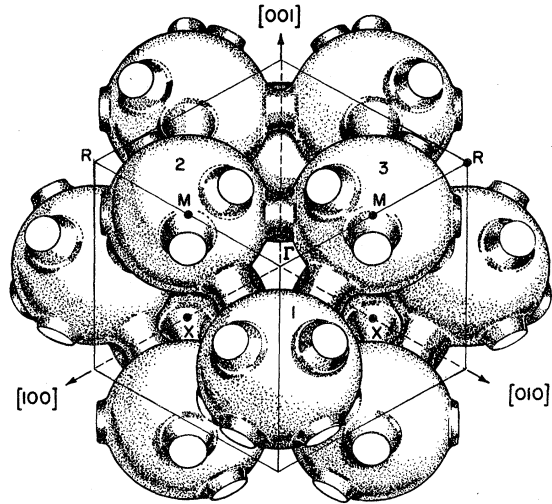


FIG. 3. Proposed topology for the large Fermi-surface piece in URh₃. Large ball-like surfaces centered at the M points in the Brillouin zone are connected by necks in $\langle 110 \rangle$ directions which would be intersected by the line S between the points X and R .

While not inconsistent with the above topology, they were inconclusive because of the very large effective masses.

Much of the dHvA data can be explained with the above topology. There are three inequivalent ellipsoids in the Brillouin zone, labeled 1, 2, and 3 in Fig. 3. With \hat{H} in the $(\bar{1}10)$ plane, only ellipsoid 1 has an extremal cross-sectional area for an orbit centered at M . Ellipsoids 2 and 3 are degenerate and support only open extremal orbits for \hat{H} along a general direction in the $(\bar{1}10)$ plane. Thus only one frequency (β_1) is expected and only one is observed in the (110) plane. The orbit is interrupted for a range of angles around [111] where it intersects necks connecting ellipsoid 1 with ellipsoids 2 and 3. In the (010) plane the three ellipsoids are all nondegenerate, so that one expects three branches each over a limited range of angles. While three branches are actually observed, only β_1 and β_2 can be clearly identified with the ellipsoids. The β_3 orbit must disappear several degrees before [101]. While the branch labeled ϵ does disappear 5° from [101], it seems to reappear for \hat{H} exactly along [101]. We will come back to this problem later.

The branch labeled ν_2 , on the basis of the proposed model, corresponds to a neck-centered orbit which includes the two ellipsoids on each side of the neck. It appears for only a short range of angles where the orbit does not run into other necks. Essentially ν_2 is a continuation of ν_1 as it reappears from behind the necks.

According to the proposed model, two hole or-

bits should exist for \hat{H} near [111]. The first is centered along the Γ - R line and traverses the three inequivalent ellipsoids and the three necks connecting them. This orbit we identify with the frequency branch ρ in Fig. 1. The large range of angles over which ρ exists can be explained if the necks are not round but have an ellipsoidal cross-section with the semimajor axes along [110]-type directions. The second hole orbit is centered at Γ and traverses six ellipsoids and the necks connecting them. No frequency branch has been observed corresponding to this much larger orbit. However, because this orbit may have a very high effective mass, we do not feel this discrepancy is serious.

For \hat{H} along [100], there should exist two hole orbits, one centered at X and one at R . From the band calculations, the orbits have quite different shapes: The R -centered orbit is a four-cornered rosette, while the X -centered orbit is more nearly circular. The relative areas of the two orbits are difficult to estimate, but they appear to be comparable, with the R -centered orbit either larger or smaller depending on which potential is assumed. The area of the X -centered orbit was roughly independent of the potential used. The anisotropy of the two orbital areas may be quite different owing to the different environments of the X and R points. The X point is surrounded by four ellipsoids whose centers are equidistant and all in the (100) plane. The R point is surrounded by six equidistant ellipsoids, four in the (100) plane and two directly above and below R on the cube edge. (The symmetry of the two points is also different. R has full cubic symmetry and the R - M line has fourfold symmetry, while X has D_{4h} symmetry and the M - X line is only twofold.) The area of the X -centered orbit is expected to increase smoothly and finally disappear as \hat{H} is tilted away from [100] in either the (100) or (110) planes.

The R -centered orbit may behave quite differently due to the two additional ellipsoids. For \hat{H} along [001], the orbit passes along four ellipsoids (two of these are labeled 2 and 3 in Fig. 3; the other two are not shown) and the necks connecting them. As \hat{H} is tipped away from [001] in the $(\bar{1}10)$ plane, the orbit passes along the lower part of the neck connecting ellipsoids 2 and 3, across two necks connecting ellipsoids 2 and 3 to the two ellipsoids not shown, and across the upper part of the neck which is not shown. At some angle from [001], the orbit could begin to pass from 2 to 3 via ellipsoid 1 and the necks connecting 2 to 1 and 1 to 3. This could produce a discontinuous increase in the area of the orbit. After a further increase in angle, the orbit could begin to pass along the outside

surfaces of the necks connecting ellipsoids 2 and 3 with those not shown, i.e., along the surface farthest from R rather than the surface closest to R . At the same time, the orbit could enclose rather than exclude the necks connecting ellipsoids 3 and 2 to 1. This would produce a second discontinuous increase in the area of the orbit.

For \hat{H} along [100], the data show only one branch, α in Fig. 1, which can be identified with these hole orbits. In the (110) plane, the α orbit disappears at precisely the angle where ζ appears, and ζ disappears precisely where ξ appears. These three orbits are related in the manner described above and we identify all of these orbits with the R -centered hole orbit. In the (100) plane, α disappears at the same angle that ϵ appears, suggesting that ϵ may also be related to the R -centered hole orbit. However, the long angular range over which ϵ exists would then be difficult to explain. Two other possible interpretations for ϵ are presented below. The absence of the X -centered orbit could be due to a high effective mass and/or a very small amplitude.

It will be noticed that the neck frequency ν_1 is apparently not observed in the (100) plane. Moreover, ν_1 is not observed for \hat{H} exactly along [110] although it is observed within 1° of [110]. Instead, a frequency nearly equal to $3\nu_1$ is observed at [110]. The latter feature could be explained by a sharp corrugation or flute at the midpoint of the neck with a large extension in the [100]-type direction, or by an additional piece of surface which is extended in the [100]-type direction and just touches the neck at its midpoint. Such a corrugation or extra piece of surface would provide an alternate explanation for the sudden discontinuity between the area of the α , ζ , and ξ orbits in the (110) plane. Three possibilities then exist for identifying the ϵ orbit. (i) the ϵ orbit is the neck in the (100) plane. The corrugation or extra piece of surface keeps the neck area much larger in the (100) plane than in the (110) plane. The β_3 orbit does not exist owing to the shape and thickness of the necks. However, the 5° gap in neck orbit just off [110] is then difficult to explain. (ii) The ϵ orbit is part of the α orbit. (iii) The ϵ orbit is β_3 . For the last two cases, one must assume a large m^* to explain the absence of the neck orbit in the (100) plane. This is not too unreasonable in view of the fact that m^* on the orbit ν_1 is too large to measure.

The model proposed here explains qualitatively many of the observed data and agrees with the band structure described below. Because the bands could be calculated only at points of high symmetry in the Brillouin zone, detailed comparison of the model with the band structure is not possible. We

hope that more complete band calculations will explain the absence of the second hole orbit near [100] and choose between the three possibilities for the ϵ orbit discussed above.

B. Band calculations

All calculations to be reported here have been performed using the overlapping charge-density model with the Kohn-Sham-Gaspár (KSG) exchange approximation.¹⁵ They were done using the symmetrized relativistic-augmented-plane-wave (SRAPW) method^{16,17} for a lattice parameter of 7.542 a.u.

The computer code used had previously been constructed and used to study the band structure of LaSn₃.¹⁸ For this study, it was necessary to expand the number of basis functions used and include the non-muffin-tin corrections outside the muffin-tin spheres [i.e., we used the so-called warped-muffin-tin (WMT) approximation].^{17,19} These WMT corrections were necessary as the rms deviation from a constant was roughly 0.25 Ry in all calculations. Neglect of this term would have made errors of 0.01 Ry in many matrix elements. The nonspherical terms inside the muffin-tin spheres, while smaller, are not truly negligible. They were neglected here, however, as the effort of including them far exceeds the utility of the increased precision.

The exchange parameter α was kept at KSG ($\alpha = \frac{2}{3}$) limit because it was necessary to provide a reasonable approximation for the f states in the uranium.²⁰ Fortunately, the various optimized α calculations indicate that this is not too far wrong for the Rh as well.²¹ This allowed us to fix one parameter in a model which suffers from too many parameters already.

The remaining parameters of our model arise because the calculation is not self-consistent. Thus we must select the occupation numbers of the atomic calculations performed to obtain the charge densities, which are then overlapped to construct the crystal potential. That is, we must select the assumed configurations U($f^{n_f} d^{n_d} s^{n_s}$) and Rh($d^{n_d} s^{n_s}$). We have not included the option of including U or Rh p states nor do we make the distinction between the two different j values for the d and f states. This greatly reduces the size of our parameter set, and the distinction between the radial charge density of a $d_{3/2}$ and $d_{5/2}$ or $f_{5/2}$ and $f_{7/2}$ state is finer than the adjustment of the parameters being made. (Only the radial dependence is important since the model calculation assumes spherical charge densities for each constituent.) Because it has been observed that the results are reasonably insensitive to the ionic character used (even for an ionic crystal such as MgO),²² and

because there is no basis for making any other choice, we have required the two constituents to each be neutral:

$$n_f + n_1 + n_2 \approx 6,$$

$$n_3 + n_4 \approx 9.$$

With this restriction, the model is still a three-parameter model. However, it is possible to greatly limit the range of these parameters by a fairly simple qualitative argument. The results of such an argument are precisely what we have found empirically to best agree with the experimental data.

To do this, however, it is necessary to be able to understand the band structure. With four atoms per unit cell, this is not as easy as for one atom per unit cell. Since each uranium atom contributes six electrons to the conduction bands and each rhodium atom contributes nine, we must account for 33 electrons in the conduction bands. Further, with the uranium contributing 13 bands (seven f bands, five d bands, one s band) and each rhodium contributing six bands (five d bands and one s band), one has to be concerned with roughly 31 bands. Since these bands are all spin degenerate, they could accommodate 62 electrons. Thus we are roughly half filling the bands. As an aid to understanding this complicated system, it is very useful to note that the $L1_2$ (or AuCu₃) structure can be thought of as an fcc structure in which the corners of the cubic cell are occupied by uranium atoms and the face-centered sites by rhodium atoms. Thus, if the system were homonuclear, we would be dealing with an fcc crystal with a Brillouin zone four times as large and thus one-fourth the number of bands. Except for the f states which arise only from the uranium atoms, it is thus possible to get an initial idea of the shape of the bands by folding a suitable fcc transition-metal band structure into the simple-cubic Brillouin zone. For example, the simple-cubic line Γ - X is made up from the fcc zone lines Γ - Δ ($\frac{1}{2}$), X - Δ ($\frac{1}{2}$), X - W (twice), and the simple-cubic Γ - M line is constructed by folding the $X(2\pi/a, 2\pi/a, 0)$ (which is Γ - K plus U - X) back to Γ and repeating twice. As an illustrative example, we do this for a thorium calculation in which the f states have been fictitiously removed. This is shown in Fig. 4. To aid the reader, those bands which occur twice have been made bolder and the symmetry labels of the fcc lattice are indicated. Clearly, as the atoms are made dissimilar, the crossings will become anticrossings and the extra degeneracy of the bands will be lifted (except at high symmetry points).

With this background, we can now greatly limit the range of the occupation-number parameters.

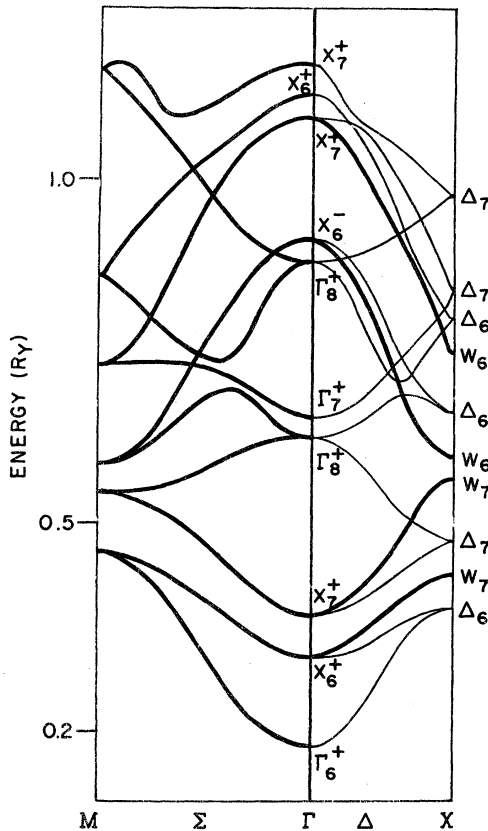


FIG. 4. Illustration of the folding back of a set of bands calculated for an fcc crystal into the form they would take for a homonuclear AuCu_3 calculation. (This particular set of bands is for a fictitious Th calculation in which the f states have been removed artificially.) The symmetry labels shown are those for the fcc Brillouin zone.

We assume that the uranium will have roughly three f states as in the pure metal. This has been checked by performing a calculation with the uranium having only two f electrons and it was found to be quite reasonable. We next note that the place where the simple-cubic zone splits up the fcc Brillouin zone is roughly the place where the plane wave states are "cut" by the d states. Thus we could expect to have roughly one band of s states, i.e.,

$$n_2 + 3n_4 \approx 2,$$

and from the neutrality requirements

$$n_1 + n_2 \approx 3,$$

$$n_3 + n_4 \approx 9.$$

If these rough arguments are taken literally, one

has reduced the number of free parameters to one.

One can even go somewhat further and assert that n_4 should be small. The f states in the system are nonmagnetic and even act as broad bands (low-density of states), which is inconsistent with the actinide-separation empirical correlation.¹⁰ Implicit in that correlation, which works amazingly well for many actinide systems, is the assumption that it is the direct interaction of the f states which produces their broadening out into bands. This is obviously not the case for URh_3 . The f states must be broadened instead by an interaction with states from the rhodium atoms. A very likely candidate for this interaction is a bond involving s and f states on the uranium and d states on the rhodium which is very strong.¹¹ One could thus expect more s character on the uranium sites and less on the rhodium sites. Again, this is precisely what we found empirically.

We have performed calculations using the five different model potentials described in Table II. As mentioned above all calculations were performed using the Kohn-Sham-Gaspár ($\alpha = \frac{2}{3}$) exchange. The calculations were performed only for the high-symmetry points and lines. This limitation was necessary as the currently programmed techniques were simply too slow to make the calculation of general points economically feasible. This can easily be understood when one realizes how large the relativistic-augmented-plane-wave (RAPW) basis set becomes in this structure. As described above, in going from the fcc to the AuCu_3 structure, one folds four points into one. This means that the basis functions used for each of the four fcc points must all be included for the one $L1_2$ point. Thus, one can predict that this structure will require the inclusion of 200 reciprocal-lattice vectors from the fact that an fcc calculation uses roughly 50. The approach used to reduce this demand has been to exploit additional symmetry. This additional symmetry, however, only exists on the high-symmetry points and lines. This prohibited a direct calculation of the

TABLE II. Configurations used in the calculations.

Calculation	Uranium	Rhodium
A	$f^3d^2s^1$	d^8s^1
B	$f^3d^2s^1$	d^9s^0
C	$f^2d^3s^1$	d^9s^0
D	$f^3d^1s^2$	d^9s^0
E	$f^3d^2s^1$	$d^{8.8}s^{0.2}$

Fermi energy and Fermi surface with our existing programs. We have therefore proceeded as follows: We first determined the approximate range of the Fermi energy using the (totally unjustified) assumption that the symmetry points and lines adequately represented the Brillouin zone. This gave us a region several electron volts wide in which we could expect the Fermi energy to fall. We then chose an energy in this region which yielded the best possible picture of the experimental situation. This is a very unsatisfactory approach which we hope to eliminate by the construction of better computational techniques. However, even using this crude approach, we are able to see a great deal about the system.

The significance of performing the number of calculations shown in Table II is that one can check for the results that are relatively insensitive to the potential employed. These are, of course, the most reliable results. With the exception of calculation C (which assumed only two f states), all calculations showed a large electron surface centered at M (see Fig. 3) with roughly the correct dimensions for the β orbits. Furthermore, these calculations showed the presence of a neck

as can be seen along the line S from X to R . In Fig. 5, we show the bands resulting from calculation B which illustrate these features. (The large electron surface can be seen from the intersections of the band with the Fermi energy along the lines Z , Σ , and T .) This then, is the most significant result of the band calculations. The various calculations (except C) are then useful in attempting to identify additional smaller pieces of Fermi surface. Of course, any Fermi surface which does not intersect a symmetry line would not be seen here. In Figs. 6 and 7 we show the energy region in the immediate vicinity of the Fermi energy for calculations D and E. From the strong sensitivity to the inclusion of rhodium s density, it is immediately obvious that calculation A (our first attempt) contained a number of obvious inadequacies and thus is not shown here. What one sees from examining Figs. 5 and 7 is that there is a strong probability that a truly self-consistent calculation would exhibit at least one Γ -centered piece and an ellipsoid along the Δ (Γ - X) line. These pieces result from some sensitive hybridizing bands, so our current calculations are inadequate to actually determine which should be pre-

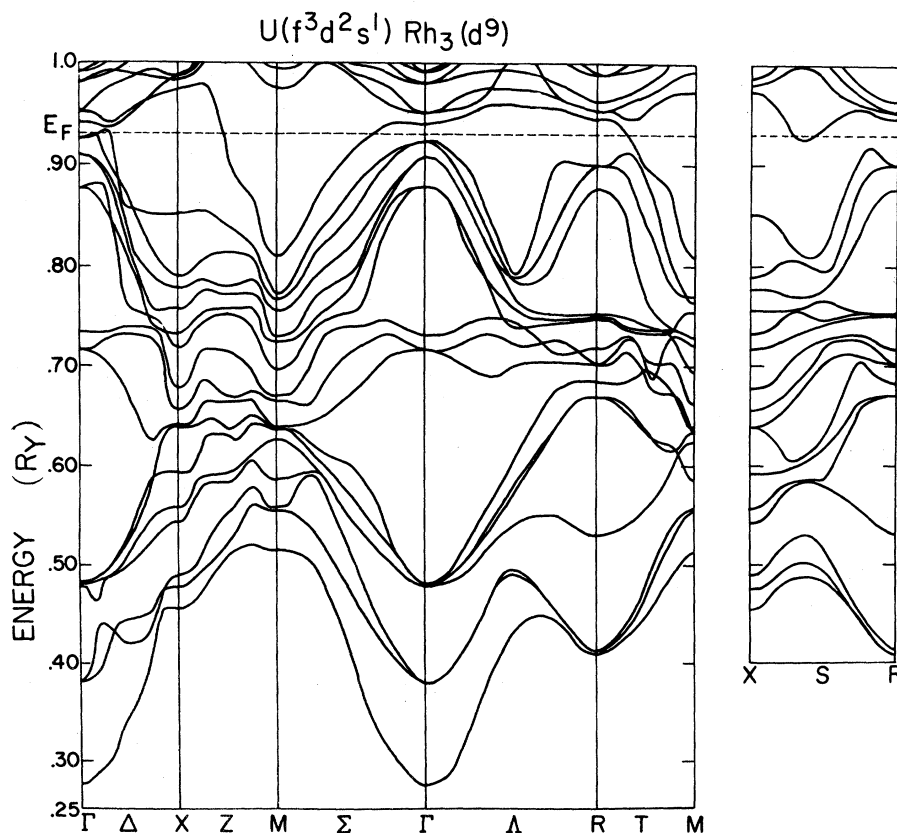


FIG. 5. Energy bands resulting from the use of potential B of Table II. Note intersection with the Fermi energy of the large Fermi-surface piece on the lines Z (X - M), Σ (Γ - M), and T (M - R) and of the neck on the line S (X - R).

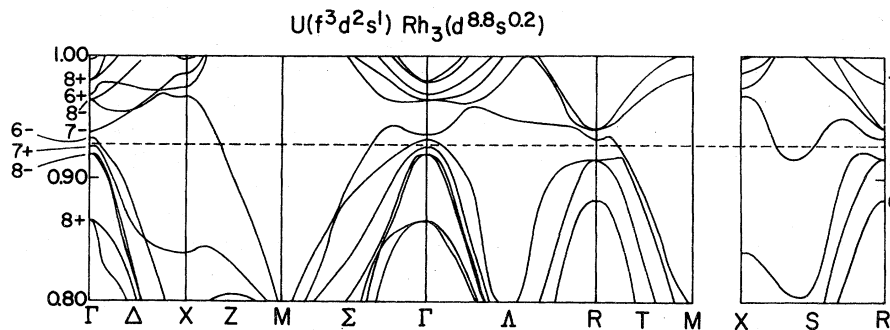


FIG. 6. Energy bands near the Fermi energy for calculation E of Table II. Note that by increasing the Rh s character used in constructing the potential, one has moved the intersection of the line T very near the point R . This would cause the α orbit to be too small. Thus one suspects that the best potential will also have little s character on the Rh. This would be consistent with a favored d - f bond formation.

dicted.

Calculation C (Fig. 8) was performed to test our assumption that the uranium should contribute three f states. We thus performed calculation C with the assumption that the uranium should contribute only two f states. Two things emerge: (a) No adjustment of E_F will give any reasonable picture of the Fermi surface. (b) The band structure implies far more than three f states which have moved down approximately 0.25 Ry. This is surprising if one is looking for very flat f bands (as in the rare earths). Indeed, some of the f bands are fairly narrow although nowhere near as flat as in the rare earths and fall just above the energy range included in Figs. 5 and 6. (They are even more cluttered than that already shown in the figures and are unoccupied.) However, some of the f states are participating in bonding and are broadened out. This is much more easily seen using the symmetry labels which are available in an (SRAPW) calculation.

IV. CONCLUSION

This work represents an initial step at opening a new level of analysis of the electronic structure

of actinide intermetallic compounds in that it brings traditional Fermi-surface probes to bear on the problem. It has shown that for at least some of these systems it is possible to obtain accurate, detailed data by extending the experiments to higher fields and lower temperatures. These results corroborate the model derived to explain the bulk property data from URh_3 . The T^3 resistivity temperature dependence and the temperature-independent susceptibility have been explained by the hybridization of the $5f$ electrons into broad bands.

The experimental results for URh_3 presented here are reasonably complete. The theoretical analysis is but an initial step. It has been adequate to serve as an aid in sorting out the experimental data but is nowhere near the type of analysis that is routinely performed for the transition elements. Work is under way to improve this situation. The first step is to develop the capability to deal economically with the full Brillouin zone rather than being limited to the symmetry lines and points. The creation of an interpolation scheme has been rejected both because the complexity of the system will make it of marginal utility and because it is

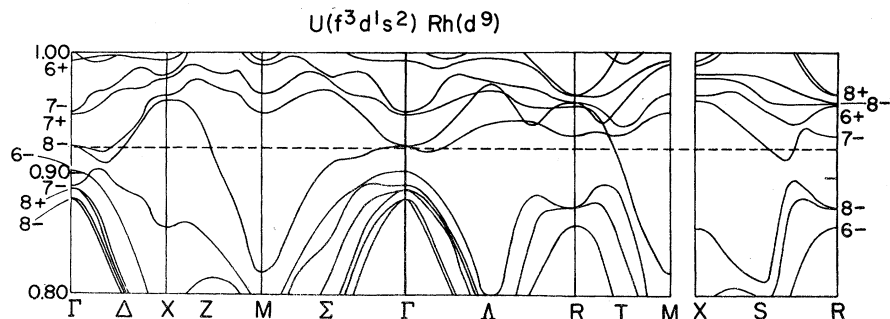


FIG. 7. Energy bands near the Fermi energy for calculation D of Table II. Note that one of the primary effects of shifting an electron from a d to an s state in the uranium atomic configuration is to shift the neck toward the R point.

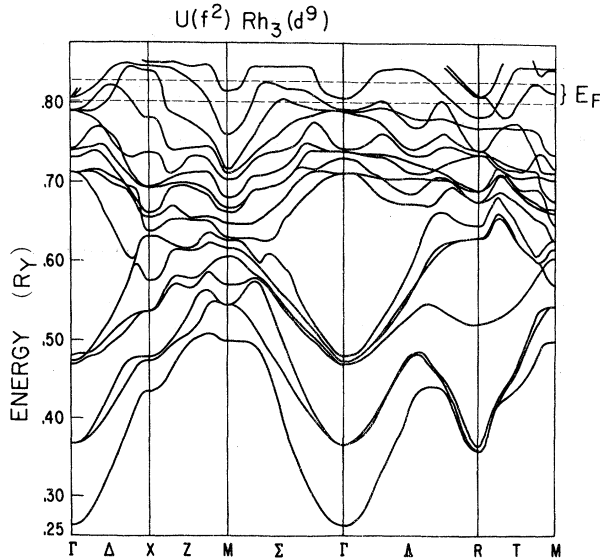


FIG. 8. Energy bands resulting from a decreased f character used in constructing the potential. (Calculation C of Table II.) Note additional f bands in the band structure. An energy range is shown for the possible Fermi energy. However, it is not possible to make even qualitative contact with the experimental data using this band structure.

obviously going to be necessary to take the second step of going to self-consistency. The requirement that one eventually go to self-consistency is easily seen from the sensitivity exhibited in Figs. 5-8. Of course, this development of full calcula-

tional capability in these systems is a necessary bridge since once one has developed some understanding of the Fermi-surface properties, one can conceive of trying to understand the wealth of other data already available in the actinide systems.

From the experimental point of view there are a number of useful areas of investigation open at this time. The most unique aspect of actinide intermetallic compounds is the existence of abundant nearly magnetic phenomena which result from narrow f -electron bands at the Fermi level. An understanding of these materials is essential in comprehending the smooth transition from nonmagnetic to magnetic behavior in metals. Some of these materials (e.g., UGe_3 and USi_3) have an electronic-specific-heat²³ γ value sufficiently low (<20) that they are excellent prospects for a dHvA study with presently available equipment. However, since even URh_3 proved to be at the edge of feasibility for some orbits, it will be even more challenging for some of the more exotic systems. Indeed our present field of 130 kG may prove to be insufficient.

In another direction, a study of UIr_3 may prove very fruitful. The lattice constant of UIr_3 is slightly larger than that of URh_3 so that the larger uranium-uranium separation yields smaller f orbital overlap and consequently would imply narrower bands in the absence of bonding. And yet the opposite appears to be the case on the basis of a measurement of resistivity which shows a T^5 increase at low temperatures.²⁴ Again it is expected that f - d bonding plays a pivotal role, and a knowledge of the band structure of UIr_3 is essential to the understanding of the problem.

†Work performed under the auspices of the U. S. Energy Research and Development Administration.

¹For a thorough review, see *The Actinides: Electronic Structure and Related Properties*, edited by A. J. Freeman and J. B. Darby (Academic, New York, 1974).

²R. Jullien, E. Galleani d'Agliano, and B. Coqblin, *Phys. Rev. B* **6**, 2139 (1972).

³A. J. Freeman and D. D. Koelling, in Ref. 1, p. 51, and references therein.

⁴A. C. Thorsen, A. S. Joseph, and L. E. Valby, *Phys. Rev.* **162**, 574 (1967); D. J. Boyle and A. V. Boyle, *Phys. Rev. Lett.* **22**, 461 (1969); R. P. Gupta and T. L. Loucks, *ibid.* **22**, 458 (1969); D. D. Koelling and A. J. Freeman (unpublished).

⁵J. E. Schirber, A. J. Arko, and E. S. Fisher, *Solid State Commun.* (to be published).

⁶M. B. Brodsky, A. J. Arko, A. R. Harvey, and W. J. Nellis, in Ref. 1, pp. 185-264.

⁷W. J. Nellis, A. R. Harvey, and M. B. Brodsky, *AIP Conf. Proc.* **10**, 1076 (1973).

⁸A. J. Arko, R. J. Trainor, M. B. Brodsky, G. P.

Sykora, and W. J. Nellis (unpublished).

⁹R. J. Trainor (private communication).

¹⁰H. H. Hill, *Nucl. Metall.* **17**, 2 (1970).

¹¹J. C. Eisenstein, *J. Chem. Phys.* **25**, 142 (1956); S. F. A. Kettle and A. J. Smith, *J. Chem. Soc. A* **1967**, 688 (1967).

¹²A. J. Arko (unpublished).

¹³R. W. Stark and L. R. Windmiller, *Cryogenics* **8**, 272 (1968).

¹⁴L. R. Windmiller, J. B. Ketterson, and J. C. Shaw, Report No. ANL-7907 (National Technical Information Service, U. S. Dept. of Commerce, Washington, D.C., 1972).

¹⁵W. Kohn and L. J. Sham, *Phys. Rev.* **140**, A1333 (1965); R. Gaspár, *Acta Phys. Acad. Sci. Hung.* **3**, 263 (1954); J. C. Slater, *Phys. Rev.* **81**, 385 (1951); Quarterly Report of the Solid State and Molecular Theory Group, MIT No. 58 (MIT, Cambridge, Mass., 1965), p. 5.

¹⁶T. L. Loucks, *The Augmented Plane Wave Method* (Benjamin, New York, 1967).

¹⁷D. D. Koelling, *Phys. Rev.* **188**, 1049 (1969).

¹⁸A. J. Freeman and D. D. Koelling, *J. Phys. (Paris)* C 3, 57 (1972).

¹⁹D. D. Koelling, A. J. Freeman, and F. M. Mueller, *Phys. Rev. B* 1, 1318 (1970).

²⁰See Ref. 3 for a discussion of the exchange approximation in the actinides.

²¹E. A. Kmetko, *Phys. Rev. A* 1, 37 (1970).

²²P. F. Walsh and D. E. Ellis, *Phys. Rev. B* 8, 5920 (1973).

²³K. H. J. Burchow and H. J. van Daal, *AIP Conf. Proc.* 5, 1464 (1971).

²⁴M. B. Brodsky and A. J. Arko (unpublished).